Self-Assembly of Graphene Oxide Nano-flakes in Lipid Monolayer at Air-water Interface

Priya Mandal[1], Rajendra P Giri[2], Bridget M Murphy[2,3] and Sajal K Ghosh[1]*
[1]Department of Physics, School of Natural Sciences, Shiv Nadar University, Gautam Buddha Nagar, Uttar Pradesh 201314, India

[2]Institut für Experimentelle und Angewandte Physik, Christian-Albrechts-Universität Zu Kiel, 24098 Kiel, Germany

[3]Ruprecht Haensel Laboratory, Christian-Albrechts-Universität zu Kiel, 24098 Kiel, Germany

Corresponding author: sajal.ghosh@snu.edu.in

ABSTRACT: The graphene family, especially graphene oxide (GO) has captured increasing prospects in the biomedical field due to its excellent physicochemical properties. Understanding the health and environmental impact of GO is of great importance for guiding future applications. Although their interactions with living organisms are omnipresent, the exact molecular mechanism is yet to be established. The cellular membrane is the first barrier for a foreign molecule to interact before entering into the cell. In the present study, a model system consisting of a lipid monolayer at air-water interface represents one of the leaflets of this membrane. The surface pressure-area isotherms and advanced synchrotron X-ray scattering techniques have been employed to comprehend the interaction by varying the electrostatics of the membrane. The results depict strong GO interaction with positively charged phospholipids, weak interaction with zwitterionic lipids and interestingly negligible interaction with negatively charged lipids. GO flakes induce significant changes on the out of plane organization of positively charged lipid monolayer with a minor influence on in-plane assembly of lipid chains. This interaction is packing specific and the influence of GO is much stronger at lower surface pressure. Even though for zwitterionic phospholipids, the GO flakes may partly insert into the lipid chains, the X-ray scattering results indicate that the flakes preferentially lie horizontal underneath the positively charged lipid monolayer. This in-depth structural description may pave new perspectives to scientific community for the development of GO-based biosensors and biomedical materials.

KEYWORDS: Langmuir monolayer, graphene oxide, lipid membrane, X-ray scattering, electrostatic interaction

1. INTRODUCTION

Graphene-based nanomaterials are extensively explored due to their diverse range of applications from optoelectronics to biomedical field.[1-2] Graphene oxide (GO), an oxidized form of graphene, holds a one-atom-thick structure similar to graphene but possesses plenty of oxygen-containing functional groups, such as carboxyl on the edges and hydroxyl and epoxy on basal plane.[3] In particular, GO has gained tremendous attention due to reliable aqueous dispersibility and colloidal stability which facilitate its applications in biosensing,[4] bioimaging,[5] drug delivery,[6] near-infrared photothermal treatment of cancers and Alzheimer's disease,[7-8] and antibacterial activities.[9-10] However, the lack of understanding of interaction between GO and biological milieu has hindered its progress in biomedical applications.[11] As any foreign molecule has to interact first with the cellular membranes, consisting mostly of phospholipids, before entering the cell, it is primarily important to understand the phospholipid membrane-GO interaction.[12]

Since the revolutionary discovery of graphene and its derivatives by Geim and Novoselov in 2004,[13] many efforts have been devoted in exploring the biological applications of these materials.[7-8, 14-15] For instance, Wu et al. revealed the nature of interaction between graphene oxide and lipid membrane by surface-enhanced infrared absorption spectroscopy (SEIRA).[16] They have concluded that hydrogen bonding, as well as hydrophobic and electrostatic interactions of choline group, dominates the adsorption of GO onto lipid membrane. By computational simulations, Chen et al. have demonstrated that graphene can easily penetrate into the bilayer due to hydrophobic interaction with lipid tails. However, GO may not enter into the membrane, rather, prefer to stay at the water-membrane interface due to hydrophilic interaction between the oxygen functional groups and lipid heads.[17] They have also commented that small size of GO flakes can pull lipids out of the membrane resulting pore formation while larger GO flakes lay flat in the middle of the membrane. In another MD simulation work, Puigpelat et al. systematically varied the size, degree of oxidation and initial orientation of graphene flakes to elucidate their effects on phospholipid membrane.[18] All these studies have mainly focused on interaction of GO with zwitterionic phospholipid membrane where the electrostatic repulsion between the phosphate group and GO is overshoot by the electrostatic attraction between the GO and choline group, and the hydrophobic attraction between them.[19]

There are few reports where researchers have investigated if the expected electrostatic attraction between negatively charged GO and oppositely charged membrane can dominate the interaction

between them. In this regard, by quartz crystal microbalance dissipation (QCM-D) technique, Frost et al. reported that anionic GO adsorbs on positively charged lipid membranes but not on negatively charged lipids.[20] Using surface pressure-area isotherm measurements, Li et al. demonstrated that head groups of lipids mainly control the interaction of GO with lipids.[21] In our recent study, using advanced X-ray scattering techniques we have revealed the structural details of interaction between GO and zwitterionic lipid using a multilayer lipid system in a controlled humid environment.[22] Experimental results show that few GO flakes can attach to the lipid heads due to hydrophilic interaction whereas some of the flakes are destined to penetrate into the interior of membrane due to favorable hydrophobic interaction between graphitic sites of GO and lipid hydrocarbon chains. Despite having several qualitative studies, molecular-level entanglements and interaction model of the GO flakes with different kinds of membranes and their structural modulations are yet to be established and verified experimentally.

Because of their amphiphilic nature, phospholipid molecules form a self-assembled monolayer at air-water interface attaching the hydrophilic heads to water and projecting their hydrocarbon chains into the air. This assembly of lipids on the 'soft' water cushion is highly representative as a leaflet of a cellular membrane due to the in-plane diffusive nature of lipids.[23-24] Hence, studying the interaction of GO flakes with a phospholipid monolayer acting as a model membrane is an important step to comprehend the interaction of these flakes with a biological membrane. Here, we aim to understand the charge and amphiphilicity dependent phospholipid membrane interaction with GO at sub-nano scale resolution. The monolayer phase behavior and structural details have been quantified by combining surface pressure-area isotherms *in situ* with X-ray reflectivity (XRR) and grazing incident X-ray diffraction (GIXD) measurements. The results show discerning effects of GO on the out-of-plane structure and in-plane ordering of the lipid molecules in the membrane depending on their head group charge and surface packing. In addition, the self-assembly of GO nano-flakes in and around the lipid layer has been evaluated.

2. MATERIALS AND METHODS

2.1. Materials

Zwitterionic 1,2-dipalmitoyl-sn-glycero-3-phosphocholine (DPPC), negatively charged 1,2-dispalmitoyl-sn-glycero-3phospho-(1'-rac-glycerol) sodium salt (DPPG) and positively charged 1,2-distearoyl-sn-glycero-3-ethylphosphocoline chloride salt (DSEPC) lipids were purchased from

Avanti Polar Lipids (Alabaster, AL) in powder form and used without further purification. DPPC and DPPG contain 16 carbons in each hydrophobic tail while DSEPC contains 18. Spectroscopic grade solvents methanol and chloroform were purchased from Sigma Aldrich whereas H_2SO_4, $KMnO_4$ and H_2O_2 were purchased from Fisher Scientific. Graphene oxide (GO) nano-flakes were synthesized from pure graphite powder by modified Hummer's method which has been described in earlier works.[25-26] As reported recently, the lateral size of GO flakes are around 180-200 nm and there is ~ 30 atomic percentage of oxygen in the synthesized GO flakes confirmed by XPS studies.[22] De-ionized (DI) water (Milli-Q, Millipore) with resistivity ~ 18.1 MΩ-cm and pH ~ 7.0 was used in preparing all samples. At this pH, the Zeta potential measurement has reported the lipid layer of DPPC to be slightly positive[27] while the presence of a few mol% of an anionic lipid into the layer provides a negative Zeta potential.[28] Similarly, a cationic lipid makes the layer positively charged at this pH.[29] Therefore, for the chosen experimental conditions, the lipid layers of DPPC, DPPG and DSEPC are, respectively, expected to be slightly positive, negative and strongly positive. The chemical structure of the lipids and the GO molecules are shown in Scheme 1.

2.2. Methods

2.2.1. Surface pressure-area isotherms: For monolayer experiments, DPPC and DSEPC were dissolved in chloroform whereas chloroform: methanol mixture (9:1 v/v) was used to prepare DPPG solution. The final lipid concentration was maintained at 0.5 mg/ml. An aqueous dispersion of 1 mg/ml GO was prepared by ultrasonication for half an hour in a cold-water bath which was then diluted to obtain the desired concentrations. Surface pressure-area isotherms from lipids were recorded using a Langmuir trough of size 55× 15 × 0.5 cm^3 (APEX, India). For the isotherms of pure lipids, 100 µl lipid solution was taken in a Hamilton syringe and spread uniformly on the water surface. Then it was left for 15-20 minutes to evaporate volatile solvents and stabilize the lipid monolayer. Double barriers were compressed symmetrically with a speed of 3.25 $Å^2$/molecule/min while surface pressure was being recorded using a Wilhelmy balance. To study the interaction of GO flakes with lipid monolayers, the flakes were dispersed in water to the chosen concentration. Then the trough was filled with this GO aqueous dispersions and the dissolved phospholipids were spread on the surface of this mixture. The surface pressure was varied to obtain the desired isotherms. All the experiments were performed at the subphase temperature of 22±1°C.

2.2.2. X-ray scattering experiments: Synchrotron-based X-ray scattering experiments are very powerful non-destructive techniques to probe the structure of lipid monolayers at air-water interface.[30-33] All the measurements were carried out at an X-ray energy of 18 keV with a beam size 0.1 × 0.4 mm (V × H) at the LISA instrument[34] in P08 beamline at PETRA III (DESY, Hamburg, Germany). A Langmuir trough, equipped with a Wilhelmy paper balance and a single movable Teflon barrier, was mounted on the diffractometer. To reduce the background scattering, the enclosure of the trough was flushed thoroughly with He with a maintained oxygen level of ~ < 0.7% and to reduce the beam damage sample was moved laterally perpendicular to the beam by 2 mm after each measurement. The X-ray reflectivity (XRR) and grazing incidence X-ray diffraction (GIXD) data were recorded from Langmuir monolayers maintained at 22.0±0.5ºC at a constant surface pressure using a LAMBDA GaAs detector placed 1.2 m from the sample providing a lateral and out-of-plane resolution of 0.0084 $Å^{-1}$. The absolute XRR profile was obtained by subtracting the background followed by normalization with respect to incident beam flux. The profile was measured as a function of wave-vector transfer, $q_z = 4\pi sin\theta/\lambda$ in the range of 0.01-0.8 $Å^{-1}$, where, θ is the incident angle. The detail of data extraction has been explained in supporting information (Figure S1). As the specular reflected beam contains mainly backscattered intensity, it affords information about layer thickness i.e., the length of hydrophilic head and hydrophobic alkyl chain of lipids projected normal to the air-water interface, electron density and roughness of the surface and interfaces.[35] The reflectivity curves were fitted using Parratt's recursive method[36-37] to determine the average electron density profile along the surface normal.[38] The XRR data analysis scheme has been explained in supporting information and a schematic has been shown in Figure S2 where different slabs of particular thickness, electron density and roughness have been considered. An infinitely large water layer of electron density 0.334 $e^-/Å^3$ and interfacial roughness 3 Å has been considered as the subphase with its parameters being constant for all the samples.

The grazing incidence X-ray diffraction (GIXD) experiments provide structural information about lateral ordering and packing of the molecular layer at air-aqueous interface.[32] In GIXD, as the angle of incidence is very close to critical angle, most of the incident beam is reflected and only an evanescent wave can travel through the sample which indeed enhances surface sensitivity.[39-40] In present experiment, the angle of incidence was kept fixed at 80% of critical angle of the air-water interface. The 2D contour spectra were obtained by varying the angle between incident and

diffracted beam, 2θ on the horizontal plane (xy plane) which is shown in Figure S3. Diffraction peaks were obtained from the 2D detector image by integrating the scattering intensity along q_z and plotted against q_{xy}. The extracted data were fitted using a Lorentz function to construct a 2D lattice formed by the lipid molecules at the air-water interface and to study their distortions in presence of GO flakes. The Bragg rods obtained by integrating the 2D intensity along q_{xy}, revealed information about tilt angle (τ) and coherence length (L_c) of alkyl tails. Due to the powder-like arrangements in 2D, the q_x and q_y components cannot be separated and hence, the data has been plotted as a function of q_{xy} [$=(q_x^2 + q_y^2)^{\frac{1}{2}}$]. Assuming a 2D hexagonal arrangements of the lipid molecules at the air-water interface[41-42] the lattice parameter can be calculated as follows:

$$d_{hk} = 1 \Big/ \sqrt{\frac{h^2}{a^2} + \frac{k^2}{b^2}} \quad (1)$$

where, $d_{hk} = 2\pi/q_{hk}$ and h, k are the Miller indices required to calculate the unit cell parameters of the in-plane lattice. The 2D crystalline coherence length (L_{xy}) was calculated from Scherer formula,[43-44]

$$L_{xy} = 0.9 \times 2\pi/FWHM_{intrinsic}\ (q_{xy}) \quad (2)$$

where the full width at half maxima (FWHM) of a peak is calculated from, $FWHM_{intrinsic}(q_{xy}) = \sqrt{FWHM_{expt}(q_{xy})^2 - FWHM_{reso}(q_{xy})^2}$, $FWHM_{expt}(q_{xy})$ being the value obtained from the Lorentzian fit of the respective peak and the $FWHM_{reso}(q_{xy})$ is the instrument resolution (0.0084 Å^{-1}). The presence of one out-of-plane Bragg rod gives rise to a molecular tilt towards nearest neighbor (NN) which is calculated by,

$$\tan\tau = \frac{q_z^d}{\sqrt{{q_{xy}^d}^2 + {q_{xy}^n}^2}} \quad (3)$$

Here, *'d'* and *'n'* denote the 'degenerate' and 'non-degenerate' peaks, respectively.

3. RESULTS AND DISCUSSION

3.1. Interaction of GO flakes with lipid monolayers at air-water interface

The surface pressure (π)–area (A) isotherm measurements are simple yet powerful method to study the surface activity and phase behavior of amphiphilic molecules that form a monolayer at air-

water interface.[45-49] The π-A isotherms are obtained by recording the change in surface pressure as a function of mean molecular area at a particular compression rate. Figure 1 shows the π-A isotherms recorded from the monolayers of DPPC, DPPG and DSEPC at air-water interface with varying GO concentrations in the aqueous subphase. All the monolayers pass through a gaseous phase where the pressure remains zero due to the absence of any inter molecular interaction. Then a liquid expanded (LE) phase is observed that transforms to liquid condensed (LC) phase with a plateau region in between exhibiting the region of coexistence of these two phases. The LC phase finally reaches to condensed phase and collapses. It is to be noted that there was no considerable surface pressure built up on compressing the trough barriers at air-GO aqueous interface in absence of any lipids. The π-A isotherm of zwitterionic lipid DPPC spread on the water surface without any GO dissolved in the subphase (Figure 1(a)) consists of several distinct phases and has been well-studied earlier.[50-51] In presence of GO dissolved in aqueous subphase, the π-A isotherm shows slight deviation, especially at higher surface pressure. The LE-LC transition pressure is shifted to a higher value of ~ 8 mN/m in comparison to the pure water. The overall isotherm presents a lower mean molecular area at air-GO aqueous dispersion interface while it collapses almost at the same pressure. As the synthesized GO flakes are only ~ 30% oxidized and, therefore, have a considerable intact graphitic region which may result in a hydrophobic interaction with the lipid tails. Further, the negatively charged carboxyl groups at the edges of the GO flakes may have an electrostatic attraction with positively charged choline group of DPPC which minimizes the lateral repulsion between the adjacent heads of lipids, effectively, reducing the mean molecular area. The above results indicate that GO has a weak effect on molecular packing of DPPC monolayer which is in well agreement with X-ray scattering results discussed in succeeding sections.

Figure 1(b) shows the π-A isotherms collected for negatively charged lipid DPPG at air-GO aqueous interface. The isotherm of DPPG without GO dissolved in subphase exhibits a much steeper increase in surface pressure without any coexistence of LE and LC phases. Gas to condensed phase transition occurs immediately after the liftoff and the isotherm collapses at a constant pressure of around 40 mN/m. In presence of GO in the subphase, the isotherm overlaps to that of without GO, confirming that GO does not interact with the negatively charged lipid DPPG. Such a qualitative observation has already been reported earlier by Li et al.[21]

Interestingly, for positively charged lipid DSEPC, presence of GO brings a significant change in the π-A isotherm which is evident in Figure 1(c). On pure water, DSEPC forms an expanded LE

monolayer and the LE-LC transition starts comparatively at higher surface pressure of around 14 mN/m. Due to the electrostatic repulsion among the positively charged head groups, there is higher molecular area available to each lipid compared to the zwitterionic lipid DPPC. In presence of GO, the mean molecular area decreases in the region of LE phase while it increases in LC phase. Interaction of negatively charged GO flakes with positively charged lipid head groups may reduce the effective inter lipid repulsion resulting in a lower mean molecular area in the LE phase. Further, as reported by Bonatout et al.[52], the GO flakes may themselves occupy space at the air-water interface on their own because of the existence of basal graphitic regions. This, predominantly, could happen at lower surface pressure providing a relatively lower mean molecular area to a lipid. However, when the lipid film is compressed, these flakes may squeeze out of the film dissolving into the water as the lipid molecules are much more surface-active compared to the GO flakes. It is also energetically favorable for the GO flakes to lay below the lipid head group at this high surface pressure because of the strong electrostatic interaction with positively charged head groups of lipids. Such a phenomenon could leave relatively higher available area to the lipids. In presence of GO, also the LE-LC coexistence region in the isotherm becomes less prominent with the LE phase spanning over a wider range of surface pressure. The limiting area of a molecule in a closely packed condensed phase (before collapse) is obtained by extrapolation of the linear part of the π-A isotherm to zero surface pressure (see arrows in Figure 1). This area for DSEPC on pure water subphase is 60 $Å^2$/molecule. The value increases to 78 and 87 $Å^2$/molecule at 0.04 mg/ml and 0.08 mg/ml GO dissolved in subphase with a corresponding increase of 30% and 45% respectively. The significant increase in limiting area in presence of GO indicates a strong interaction of GO sheets with the DSEPC monolayer. These observations manifest that the GO flakes strongly interacts with DSEPC lipid layer compared to the zwitterionic lipid DPPC and negatively charged lipid DPPG. Therefore, we can conclude that the charge and chemical structure of lipids play a major role in controlling the interaction with GO nanosheets.

The interaction of GO with differently charged lipid monolayers is expected to alter the physical property of the layer which is quantified by calculating the in-plane elasticity using the expression, $K = -A\,(\partial\pi/\partial A)_T$. This has been calculated from π-A isotherm and shown in the inset of Figure 1. As explained by Geraldo et al., the in-plane elasticity is also termed as surface compressional modulus.[53] This in-plane elasticity provides information regarding the molecular packing and

compactness of a film. As apparent in inset of Figure 1, for zwitterionic and negatively charged lipids, the GO flakes do not influence much the in-plane elasticity of lipid films. However, GO affects significantly the value of elasticity of the positively charged lipid DSEPC. This change mainly corresponds to the modified intermolecular interactions of polar head groups, which, in turn, may influence lipid chain configuration. At a particular pressure of 20 mN/m, the elasticity of DSEPC on aqueous subphase increases from 25.5 mN/m to 68.1 mN/m in presence of 0.04 mg/ml GO in the aqueous subphase. The increase in surface elasticity indicates the rigid and well-packed structure of lipid monolayer in presence of GO. This considerable increase in elasticity or surface compressional modulus in presence of GO is expected to alter the self-assembled structure of DSEPC monolayer.

To confirm the thermodynamic stability of the lipid monolayer, a series of hysteresis experiments has been performed taking three consecutive cycles of compression and decompression. The hysteresis curves obtained from DSEPC monolayer at air-water and air-GO aqueous dispersion interface exhibit almost identical isotherms which are shown in Figures 2(a) and (b), respectively. Similar experiments with the monolayers of DPPC and DPPG almost reproduce the isotherms over the cycles (Figure S4). This confirms the formation of stable and reversible monolayer in absence and presence of GO in the subphase. At least within the given range of pressure and time, there is no considerable loss of molecules during the isotherm measurements shown in Figure 1.

In order to find out the stability of pre-compressed monolayers, the lipid solutions are spread uniformly on the subphase using a Hamilton syringe until it reaches a fixed surface pressure of 20 mN/m and the corresponding changes in surface pressure are monitored as a function of elapsed time. Figure 2(c) shows surface pressure-time stability curve of DSEPC monolayer at air-water interface (black curve) which is sufficiently stable over the period of ~ 3 hrs. The measurements for DPPC and DPPG lipids are shown in Figure S5. These data confirm the stability of the monolayers and validate the results obtained in X-ray scattering experiment discussed in the following section.

The adsorption of GO into the DSEPC monolayer formed at air-water interface has been studied at a surface pressure of 20 mN/m which is shown in Figure 2(c). An amount of 1 mg/ml GO dispersion is carefully and slowly injected underneath the monolayer so that the final concentration of GO reaches to 0.04 mg/ml with respect to the whole subphase. Then, the time evolution of

surface pressure is monitored. The percentage change in the surface pressure has been calculated using the following equation,

$$\Delta\pi = \frac{\pi_f - \pi_0}{\pi_0} \times 100\%$$

where, π_f and π_0 are the initial and final surface pressures, respectively. The increase in surface pressure over time clearly indicates the strong interaction of GO with positively charged lipid which is consistent with surface pressure-area isotherm results. This significant change in surface pressure is attributed to the long-ranged electrostatic interaction of positively charged choline group of DSEPC with negatively charged carboxyl group (COO^-) of GO. It is worth noticing that there is no significant change in surface pressure of DPPC and DPPG monolayers in presence of GO in the subphase which is shown in Figure S5. These results are quite consistent with the findings reported by Li et al. earlier showing stronger affinity of GO to positively charged lipid compared to the zwitterionic and negatively charged ones.[21]

The morphology of lipid film which is dip coated on a hydrophilic Si substrate is investigated by AFM imaging. Figure 2(d) shows the uniform film of DSEPC deposited at 20 mN/m from air-water interface demonstrating the formation of homogeneous monolayer which is clearly visible in its height profile. When the LB film is transferred from air-GO aqueous dispersion interface, GO nanosheets are then visible in the morphology of the film (Figure 2(e)). The height of the GO flakes is ~1 nm which is in well agreement with our previous results confirming the organization of GO nanosheets around the positively charged lipid film.[22] The Brewster angle microscopy (BAM) images of the lipid films on the water subphase and the subphase with GO flakes dispersed in it shown in Figure S6 indicate an arrangement of the flakes below the positively charged lipid DSEPC consistent with the increased in-plane elasticity observed. In case of the DPPC and DPPG lipid films, no such arrangement is observed. A detailed description of this observation can be found in the Supporting Information**.**

3.2. GO flakes modify the structural organizations of lipids in monolayer

To gain deeper insights into the structure of lipid monolayer formed at the air-water interface and the organization of GO flakes in and around the layer, XRR and GIXD studies are carried out which are discussed in the following section.

3.2.1. GO flakes self-assemble in and around a zwitterionic lipid layer: Figure 3(a) represents the reflectivity curves obtained from DPPC monolayer at a surface pressure of 30 mN/m with the fitting parameters given in Table 1. The corresponding electron density profiles (EDPs) along with a schematic of the organization of lipid molecules are shown in Figure 3(b). In presence of 0.04 mg/ml GO in the aqueous subphase, the first dip of XRR profile is slightly shifted towards lower q_z confirming an increase in overall film thickness. The thickness of polar head and hydrophobic tail of DPPC monolayer at air-water interface is found to be 6.2 and 17.6 Å, respectively. The corresponding electron densities are 0.447 and 0.325 $e^-/\text{Å}^3$ which are in good agreement with the previous reports.[54] At GO-aqueous interface, the thicknesses of head and tail are increased by 9.7% and 1.1% while the electron density of head increased by 2.3% and that of tail decreased by 3.7% respectively. Overall changes in structural parameters suggest the flakes to insert into the lipid film. These slight changes in the parameters indicate a weak interaction between the GO and the zwitterionic lipid. DPPC is neutrally charged with a permanent dipole moment whereas GO flakes contain negatively charged carboxyl groups (COO^-) on the edges with the hydroxyls and epoxies on the basal plane. As there is no net charge in the polar head of DPPC, we may consider that the interaction of GO with DPPC is not governed by electrostatics. Rather, the hydrogen bonding, hydrophobic interaction and the van der Walls force dominate the weak interaction between them which is similar to the observations from planar protein molecules in zwitterionic membrane.

To understand the in-plane arrangements of lipids in presence of GO in the subphase, GIXD experiments were performed at a surface pressure of 30 mN/m. As is seen in Figure 3(c), two in-plane diffraction peaks are observed at q_{xy} = 1.342 Å^{-1} and 1.477 Å^{-1} for pure water subphase. The peaks can be indexed with (10) and $(1\bar{1})$ of a distorted hexagonal phase as reported earlier by Miller et al.[54] and Majewski et al.[55] For this distorted hexagonal unit cell, even though $|a| = |b|$ but $\gamma \neq 120^o$. The distortion in hexagonal lattice arises due to the collective molecular tilt in the alkyl chains, which is reflected in the Bragg rod profile (Figure 3(d)). Inter planar spacing, d_{10} = 4.68 Å and $d_{1\bar{1}}$ = 4.25 Å give rise to the lattice parameter of $|a| = |b| = 5.09$ Å and $\gamma = 113.2^o$. It provides a mean molecular area of about 47.7 Å^2.[42] The coherence length (L_{xy}) along the two crystallographic directions, (10) and $(1\bar{1})$ are found to be 70 and 234 Å respectively. In presence of GO, the diffraction peaks again provide a distorted hexagonal unit cell with dimensions $|a| = |b|$ = 5.05 Å, $\gamma = 114.5^o$ and area per molecule to be 46.3 Å^2. These parameters are close to that

obtained for pure water, thereby, suggesting a weak interaction between the GO and the lipid layer. The respective coherence lengths are found to be 67 and 279 Å. The Bragg rod analysis revealed two maxima for DPPC on aqueous surface, one at q_z ~ 0 $Å^{-1}$ (Vineyard-Yoneda peak)[56] and the out of the horizon one at q_z ~ 0.741 $Å^{-1}$ (Figure 3(d)). The presence of one out of plane Bragg rod suggests a nearest neighbor (NN) tilt of 33.5º in lipid chain measured with respect to the surface normal. The coherence length (L_z) is found to be 19.6 Å. At air-GO aqueous interface, the tilt is calculated to be 32.2º with coherence length L_z = 14.5 Å. All the numeric value extracted from GIXD data are tabulated in Table 2. The slight decrease in tilt of lipid chains in presence of GO is consistent with the little increase in thickness of tail region observed in XRR data.

3.2.2. GO flakes are repelled by a negatively charged lipid layer: As shown in Figure 4(a), the reflectivity profile of DPPG monolayer on the surface of GO aqueous dispersion is very similar to that obtained on pure water surface. The electron density profiles of the lipid layers without and with GO dissolved in aqueous subphase coincide on top of each other (Figure 4(b)) indicating a negligible influence of the GO flakes on the self-assembled structure of the lipid layer. The parameters obtained from XRR fitting are listed in Table 1. As the head group of DPPG is negatively charged, carboxyl group (COO^-) of GO sheets experiences the long-range electrostatic repulsion and hence do not reach to the lipid layer. The independent GIXD measurements have shown a similar result that is summarized in Figure 4(c) and (d). The diffraction peak registered for DPPG monolayer at air-water interface at 30 mN/m has two maxima at q_{xy} = 1.482 $Å^{-1}$ and 1.514 $Å^{-1}$ which can be indexed as (10) and ($1\bar{1}$) peaks from a distorted hexagonal lattice.[57] The lattice parameter is $|a|$ = $|b|$ = 4.83 Å with the angle γ = 118.6º providing an area per molecule = 40.8 $Å^2$. The in-plane coherence length along the two crystallographic directions are found to be L_{10} = 210 Å and L_{01} = 295 Å. Similarly, at air-GO aqueous interface, the observed diffraction peaks give rise to the same lattice with same lattice parameters (Table 2). The Bragg-rod analysis for DPPG at air-water interface revealed two maxima centered at q_z ~ 0 $Å^{-1}$ and q_z ~ 0.335 $Å^{-1}$ respectively which gives rise to a nearest-neighbor (NNs) tilt of 14.7º with respect to the surface normal and area per molecule 19.1 Å. In presence of GO, Bragg rod analysis gives identical results as obtained on pure water.

3.2.3. GO flakes self-assemble horizontally underneath a positively charged lipid layer: The reflectivity profiles obtained from the monolayer of positively charged lipid DSEPC on the water and GO dissolved-water surfaces are shown in Figure 5 with the fitted parameters in Table 1. As is readily evident from the shape and width of the Kiessig fringes, presence of GO in the subphase has a considerable effect on the assembly of the lipids at the air-water interface. The gradual shift of the first dip of reflectivity curves towards lower q_z along with the decrease in the thickness of the fringe width confirms an overall increase in the lipid-GO film thickness. Further, the dips become progressively prominent with increase in GO concentration. The profile has been modified due to the predominant layer of GO adjacent to the lipid head group. Here, the flakes can accumulate into lipid-water interface offering an electron density contrast at the interface. This prediction is established by the analysis of the data by modelling the film with three boxes (Table 1). On pure water, the thickness of head and tail of DSEPC molecule at 30 mN/m are found to be 7.0 and 18.6 Å with their respective electron densities of 0.386 and 0.329 $e^-/\text{Å}^3$. The head group electron density of DSEPC is much lower compared to that of zwitterionic DPPC on water subphase. This is probably due to the higher separation between the head groups arising from electrostatic repulsion. Higher mean molecular area of DSEPC compared to DPPC observed in the pressure-area isotherm data at this surface pressure also indicate this possibility. In presence of 0.04 mg/ml GO dispersion, the head group thickness is increased to 7.8 Å with an electron density of 0.399 $e^-/\text{Å}^3$. Interestingly, the tail thickness decreases slightly to 18.1 Å with an electron density of 0.327 $e^-/\text{Å}^3$. These results are consistent at higher concentrations of GO where at 0.08 mg/ml GO dispersion, the head group thickness is increased by 21.4% while the electron density by 7.9%. In contrast, the thickness and electron density of the tail region is decreased by 8.6% and 7.0% respectively (Table 1). This XRR result of much higher increase in thickness of the head group region compared to the chain region suggests the binding of positively charged choline group of DSEPC with negatively charged carboxyl group (COO^-) of GO. This long-ranged interaction perhaps has assisted the GO flakes to self-assemble below the lipid layer at the lipid-water interface. It matches well with the higher mean molecular area of lipids observed in isotherm measurement and the prediction made for the organization of the flakes at higher surface pressure. As can be seen in Table 1, the thickness and electron density of this layer increases with increasing concentration of GO in the water. The consistent variations in thickness and electron density of the different parts of the lipid film convincingly illustrate that the strength of interaction of GO

with positively charged lipid is higher compared to the neutral and negatively charged ones. It was observed in the isotherm study that in presence of GO, the film becomes more rigid with a higher value of in-plane elasticity compared to the pristine lipid film. The overall increase in film thickness quantified by the XRR study of the DSEPC lipid layer in presence of GO is consistent with the isotherm data. On increasing the concentration of GO in the system, the film thickness and electron density increase monotonically, confirming a structure of the film that includes the lipid film and the assembled GO flakes. This composite structure can enhance the rigidity of the film.

The GIXD patterns obtained from DSEPC lipid monolayers on water surface and GO dissolved water surface at surface pressure of 30 mN/m are shown in Figures 5(c) and (d). At air-water interface, two diffraction peaks are observed at q_{xy} = 1.463 $Å^{-1}$ and 1.504 $Å^{-1}$ which present a 2D distorted hexagonal unit cell with the lattice parameters of $|a| = |b|$ = 4.87 Å and γ = 118.1º. The area per molecule is calculated to be 41.8 $Å^2$ and the coherence lengths are 157 and 94 Å along (10) and $(1\bar{1})$ directions, respectively. The Bragg rod analysis has revealed a single peak at the horizon (q_z ~ 0 $Å^{-1}$). The absence of any peak at out of the horizon confirms the absence of molecular tilt in lipid chains. In presence of different concentrations of GO, the alkyl chains have similar ordering with almost identical lattice parameters (Table 2) which suggest the assembly of GO flakes below the head group region. Even though such an organization did not influence the in-plane organization of DSEPC molecules, it has exhibited an effect on the out-of-plane electron density profiles. Along with assembling horizontally below the lipid head group, some GO flakes may have occupied some area at the air-water interface. It can influence the electron density profile plotted along film normal as the profile is obtained by averaging the in-plane density. The small domain of GO at the air-water interface may effectively reduce the electron density of the slab taken to model the chain region. However, the presence of other GO flakes under the lipid head groups will increase the density value of the head group region.

3.3. Role of surface pressure on GO-positively charged lipid interaction

In above sections, it has been observed that GO flakes have a strong affinity to interact with positively charged lipid. Even though the data discussed above have indicated the GO flakes to lay horizontal below the positively charged lipid layer, they may also insert into the layer. The insertion of any molecules into the lipid layer highly depends on its surface pressure.[58-61]

Therefore, the interaction of GO flakes with the DSEPC lipid layer has been investigated as a function of surface pressure to confirm the organization of the flakes in and around the layer. The XRR profiles along with corresponding electron density profiles of DSEPC lipid layer on the GO-dissolved water surface (0.08 mg/ml) are shown in Figures 6(a) and (b). The measurements have been performed at the surface pressure of 10, 20, 25 and 30 mN/m. The fitting parameters are summarized in Table 3. With increase in surface pressure, the first dip of XRR profile has shifted a bit towards lower q_z, indicating an increase in film thickness. At a surface pressure of 10 mN/m, the thickness of lipid head and tail are found to be 7.6 and 14.7 Å respectively with the electron densities 0.419 and 0.329 $e^-/\text{Å}^3$. With increase in surface pressure, the thickness of tail increased with a systematic decrease in electron density. Increasing surface pressure is expected to form a more ordered chain, which is evident in the GIXD data. This can increase effective chain length providing a more volume for the chain and thereby reducing the electron density. However, the structural parameters of lipid head group remain almost unaltered with pressure (Table 3). Interestingly, the thickness and electron density of GO layer also remains unaffected while the surface pressure was increased. This is likely to happen when the GO flakes are self-assembled below the lipid layer rather than inserting themselves into the layer. Note that the vertical insertion of the GO layer with an average size of 180-200 nm is expected to be influenced by the surface pressure and finally should have shown an effect on the whole film including the lipid head and the GO layer.

The GIXD patterns obtained during DSEPC monolayer compression are shown in Figures 6(c) and 6(d). The scan in the range $1.4 < q_{xy} < 1.5$ Å^{-1} has revealed single Bragg reflection at lower surface pressure. At 10 mN/m, reflection measured at $q_{xy} = 1.465$ Å^{-1} corresponds to a hexagonally ordered lipid chain with a spacing of 4.29 Å. Presence of this single diffraction peak indicates the absence of any distortion in the hexagonal lattice (Table 4). At the highest surface pressure (30 mN/m), the distortion is observed which has already been discussed above. Physical insertion of any molecule in a lipid layer is easier at lower pressure compared to that of higher pressure, which is expected to show an effect on the lipid chain organization. As there was no such pressure dependence manifested in the GIXD data, the flakes seem to self-assemble horizontally below the lipid layer at all surface pressures as is anticipated from XRR analysis. However, at low surface pressure, some of the flakes may lay at the air-water interface on their own, as predicted from the lipid isotherm data, without inserting into the lipid film. Such an arrangement of flakes

lying in their own domain may not significantly affect the GIXD data observed from the lipid chains. Note that the GIXD data of DSEPC monolayer on pure water surface shows a similar result of independency of the parameters with pressure (Figure S7). The corresponding structural parameters are given in Table S1.

3.4. Further discussions

The interaction of GO flakes with a lipid membrane is a consequence of multiple forces. The flakes have the hydrophilic parts due to presence of carboxylic groups at the edges and phenol hydroxyl and epoxide groups at the basal plane.[62-63] As 30% of atoms are oxygen in the synthesized GO flakes, it has the hydrophobic patches due to the presence of intact carbon-carbon sp^2 domains. The possible organizations of GO-flakes in and around the lipid monolayer have been shown in a schematic presentation in Figure 7. In case of zwitterionic lipid layer, the flakes may have both hydrophilic interaction with the polar heads and hydrophobic interaction with the nonpolar hydrocarbon chain. Therefore, some of the flakes may insert into the lipid layer while other may assemble below the layer affecting whole film structure. Such a possibility has been discussed in our recent report where a zwitterionic lipid multilayer has been used.[22] The long-range Coulomb repulsion between the GO flakes and the negatively charged lipids may overshadow the attractive hydrophobic interaction, thereby exhibiting no organization of the flakes in and around the lipid layer. On other hand, the orders of magnitude stronger attractive electrostatic force may hold the GO flakes to lay horizontal below the positively charged lipids overshadowing the hydrophobic interaction. For this lipid case, at lower surface pressure, some of the flakes may lay at the air-water interface forming a phase-separated region from that of the lipid film. All these hypotheses require much more rigorous experimental evidences which may obtained from other techniques. Note that from XRR and GIXD studies, Bonatout et al. have found that the pure GO sheets, spread at air-water interface, either lie flat or orient randomly at water surface at low surface pressure. At higher surface pressure, they form a double layer.[52] Here, while one layer is in contact with water having GO sheets lying flat in water, the other one has the GO sheets tilted with respect to water surface. Such an inherent property of the orientation of the flakes, however, in the present study, have been highly influenced by the presence of lipids at the air-water interface. As the lipids are strongly surface active, the orientation of the flakes at the interface is mainly dominated by the lipids.

Graphene-based nanomaterials exhibited tremendous attention in a wide range of applications owing to their unique physicochemical properties. In last few years, particularly GO has witnessed a rapid growth in diverse fields such as biosensor, bioimaging, drug delivery and disease diagnosis.[4-5, 7-8] For the advancement of these applications, it is crucial to understand the interaction of GO with cellular membrane to comprehend its toxicity and environmental impact. Using molecular dynamics simulation, it has been reported that GO nanosheets can pull out lipids from a membrane resulting in formation of pores.[17] The graphene nanoflakes have been reported to insert into the hydrophobic core of the membrane[18] which is mainly controlled by the size and oxidation state of the flakes. In contrary, there is report that suggests a neutral phospholipid not to adsorb GO flakes.[64] Present study has shed lights on many of these issues as explained above. The acquired knowledge from this study may be useful for developing devices for biophysical applications. For example, the bio-molecular film of lipid with embedded GO-flakes deposited on a semiconductor substrate could be an excellent platform for developing field effect transistor (FET) based biosensors. Further, it has been suggested that the GO-membrane complexes can be useful to generate bacteria sensing devices, label-free DNA sensors and polyelectrolyte chemical transistors.[65] It has also been found that many of the lifesaving drug molecules highly adsorb on the GO flakes which opens up the possibility of using the flakes as drug carriers.[65] Even the GO-DNA complexes are investigated for delivering the gene materials into the cell.[66-68] In all these cases, understanding the interaction of GO with lipid membrane is a crucial step in releasing these molecules into the cellular matrix.

In the present study, a simple model membrane of lipid monolayer containing a single phospholipid component has been chosen to probe the interaction of GO with a cellular membrane. Additionally, as pH controls the electrostatic nature of interacting species, a pH dependent detailed investigation of interaction of GO with lipid films could be informative in the future. In such case, the Debye length as it depends on the types of salt and their concentrations, would be better defined. Another important aspect of future study could be the experimental verification of the cholesterol extraction capability of the GO flakes from lipid bilayer as proposed by simulation.[69] Fundamentally, the cellular membrane is a multicomponent phospho- and glycolipid system with many other macromolecules including cholesterol and trans- and peripheral membrane proteins embedded in it.[70-71] In future, a dip coated lipid bilayer on a polymer cushion could provide a

model membrane closer to nature.[72] Clearly a more component system is required in future to fully grasp the complex mechanism of interaction of GO with cellular organisms.

4. CONCLUSIONS

Electrostatic interaction of GO nanoflakes is shown to vary strongly with differently charged phospholipid head groups by surface pressure-area isotherms of the monolayers. Synchrotron X-ray scattering techniques reveal details of the molecular level structure of self-assembled organization of GO nanoflakes due to variation in the degree of interaction with differently charged phospholipid model membranes. Here, GO flakes are shown to accumulate underneath the positively charged phospholipid monolayer due to a strong interaction resulting in increased electron density and layer thickness. Interestingly, while GO exhibits a moderate effect on the zwitterionic one, it does not affect a negatively charged phospholipid monolayer. The structural details on molecular arrangement and interaction may pave the new avenues to explore and exploit GO-lipid complexes as an effective nanoscale biological interface for future bioelectronic devices.

ASSOCIATED CONTENTS

Supporting Information

X-ray reflectivity (XRR) data extraction scheme, XRR data analysis scheme, GIXD diffraction pattern, Thermodynamic stability of Langmuir monolayer, Adsorption of GO into the monolayers of DPPC and DPPG, Brewster angle microscopy (BAM) images of lipid monolayers, Table S1: Structural parameters obtained from the GIXD data of DSEPC monolayer at air-water interface at different surface pressure.

ACKNOWLEDGEMENTS

We thank the Science & Engineering Research Board (SERB), Department of Science and Technology (DST), India for funding the project (File no. EMR/20l6/006221). We acknowledge DST, India for the financial support for travel and accommodation and facilitating the parts of the experiments carried out at PETRA III, DESY (Hamburg, Germany). We thank DESY for the access to PETRA III and the beamline staff at P08 for their support. We acknowledge the research grant BMBF/05K16FK1/05K19FK2 for financing LISA instrument. P. M. thanks Shiv Nadar

University for the research fellowship. We are thankful to Mr. Ajit Seth and Mr. Prashant Hitaishi for their help in taking BAM images.

Scheme 1. Chemical structure of lipids and graphene oxide: (a) 1,2-dipalmitoyl-sn-glycero-3-phosphocholine (DPPC), (b) 1,2-dispalmitoyl-sn-glycero-3phospho-(1'-rac-glycerol) sodium salt (DPPG), (c) 1,2-distearoyl-sn-glycero-3-ethylphosphocoline chloride salt (DSEPC) and (d) graphene oxide (GO).

(a) 1,2-Dipalmitoyl-sn-glycero-3-phosphocholine (DPPC)

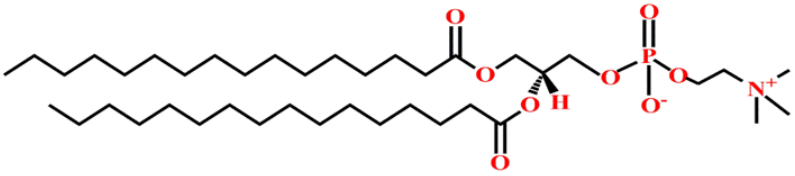

(b) 1,2-dispalmitoyl-sn-glycero-3phospho-(1'-rac-glycerol) sodium salt (DPPG)

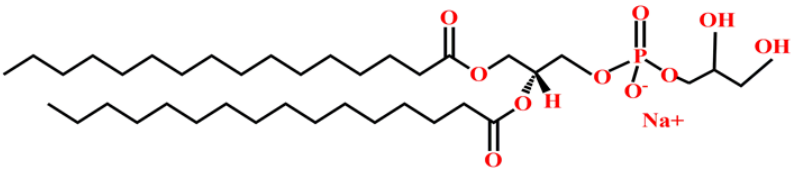

(c) 1,2-distearoyl-sn-glycero-3-ethylphosphocoline chloride salt (DSEPC)

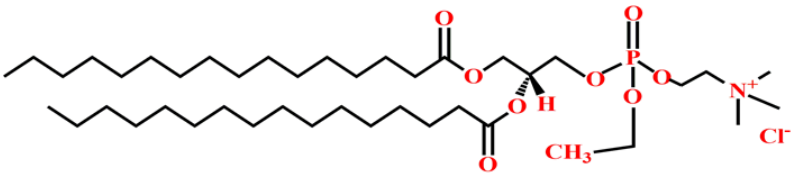

(d) Schematic of graphene oxide (GO)

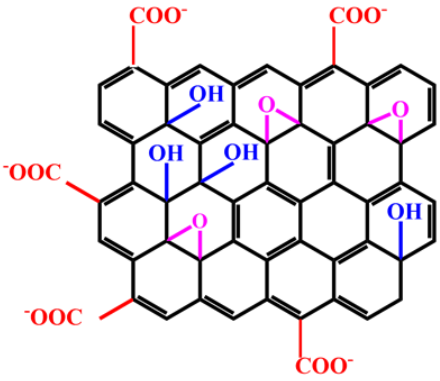

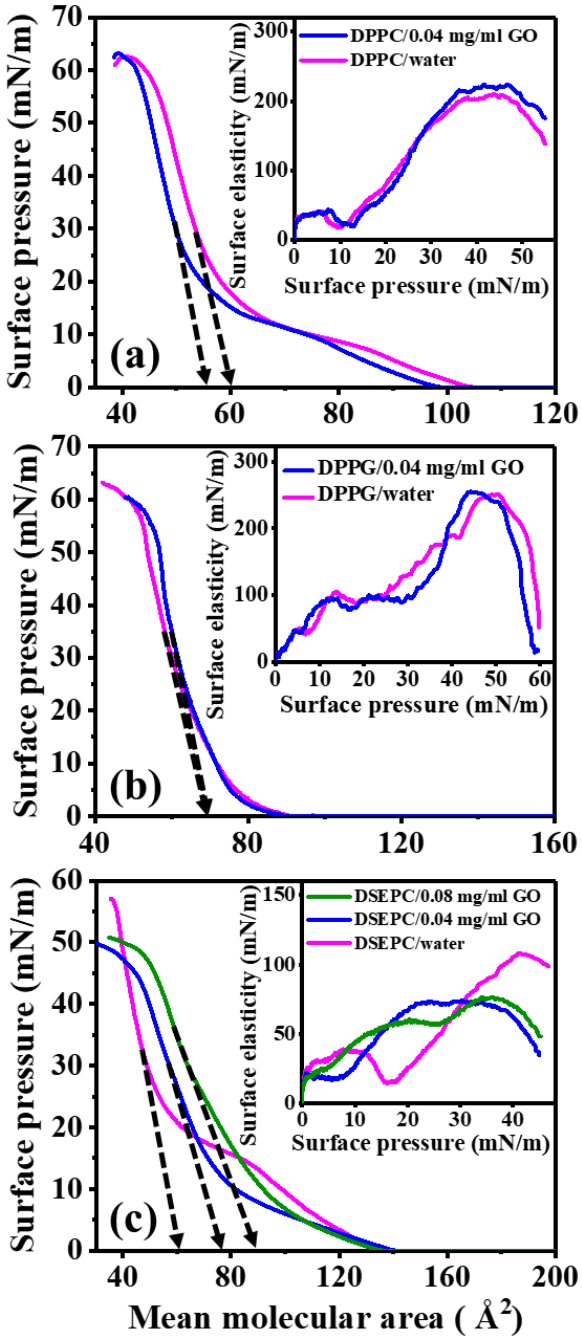

Figure 1. Surface pressure-area isotherms of lipid monolayers at air-water and air-GO aqueous interface. Isotherms of (a) neutrally charged DPPC, (b) negatively charged DPPG and (c) positively charged DSEPC. The intercepts of dashed lines with abscissa signify the limiting molecular area of a lipid in liquid condensed phase. Inset: Variation of in-plane elasticity or surface compressional modulus of lipid monolayers as a function of surface pressure. The GO aqueous dispersion of two different concentrations, namely, 0.04 mg/ml and 0.08 mg/ml have been used as the subphase. All measurements were performed at ~22^{o}C.

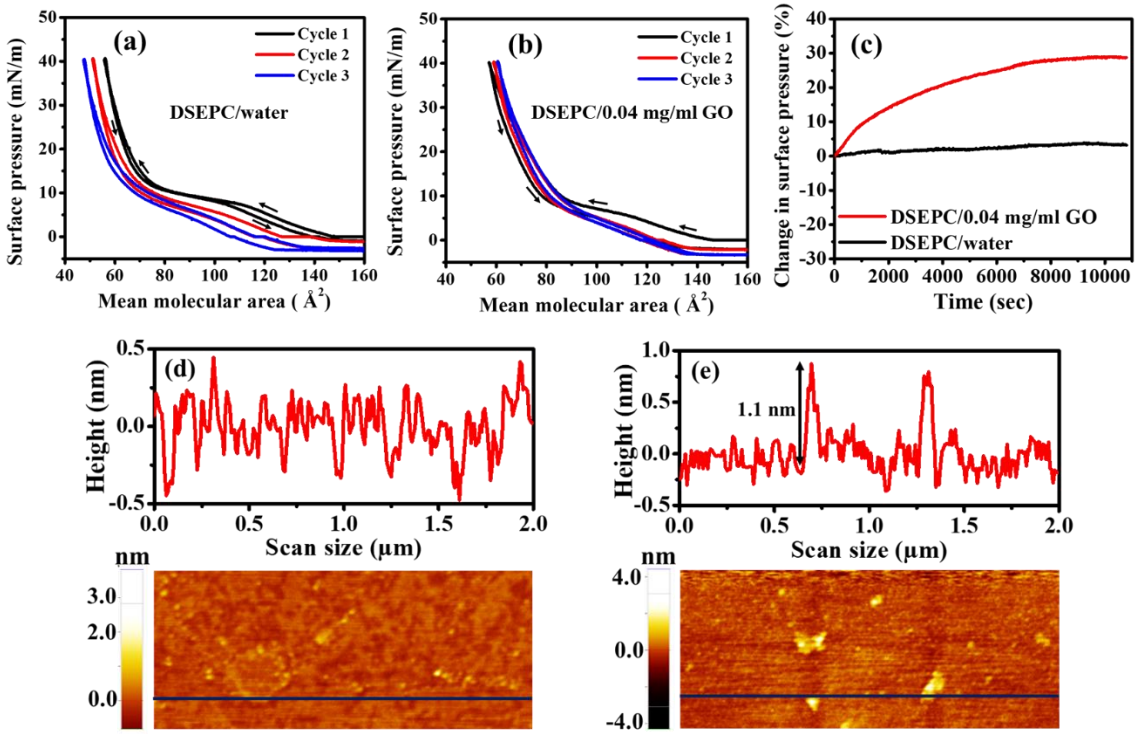

Figure 2. Cycles of compression-decompression of surface pressure-area isotherms of DSEPC monolayer at (a) air-water and (b) air-GO (0.04 mg/ml) aqueous dispersion interface. (c) Relative changes in the surface pressure vs elapsed time of DSEPC monolayer at air-water (black curve) and air-GO (0.04 mg/ml) aqueous dispersion (red curve) interface. AFM images of DSEPC monolayer transferred on a polished Si substrate from, (d) air-water and (e) air-GO (0.04 mg/ml) aqueous dispersion interface.

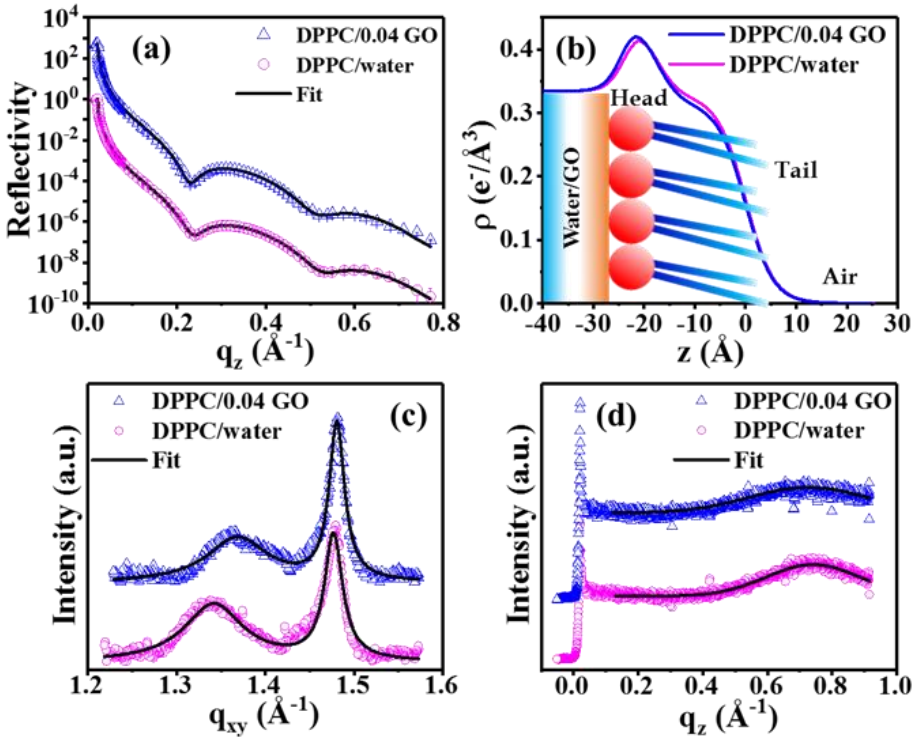

Figure 3. (a) X-ray reflectivity (XRR) profiles of DPPC monolayer at air-water and air-GO aqueous interface at a surface pressure of 30 mN/m. Symbols represent the experimental data whereas the solid lines indicate the model fits. XRR profiles were vertically offset by a factor 100 for clarity. (b) Corresponding electron density profile (EDP) obtained by fitting of XRR profiles as shown in (a). (c) Background-subtracted diffraction peaks and (d) corresponding Bragg rods obtained from GIXD experiment from the monolayer. The diffraction peaks were fitted using Lorentzian function whereas the Bragg rods were fitted using Gaussian function. All the curves have been offset vertically for clear visibility.

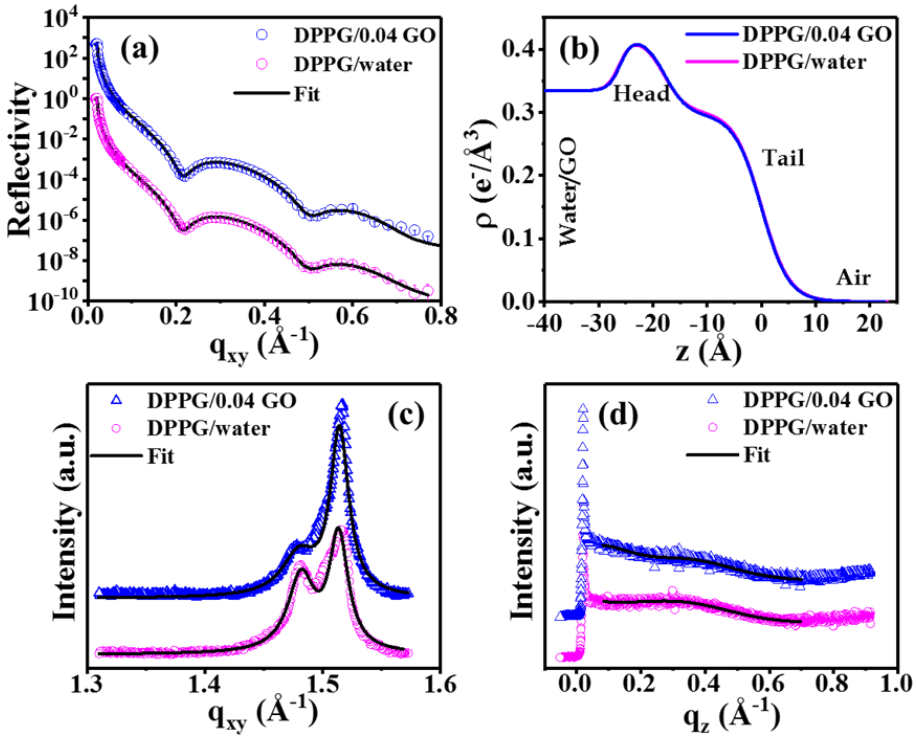

Figure 4. (a) X-ray reflectivity XRR profiles of DPPG monolayer at air-water and air-GO aqueous interface at a surface pressure of 30 mN/m. Symbols represent the experimental data whereas the solid lines indicate fits. (b) Corresponding electron density profiles (EDPs) obtained from XRR profiles. (c) Background-subtracted diffraction peaks and (d) corresponding Bragg rods obtained from GIXD experiment.

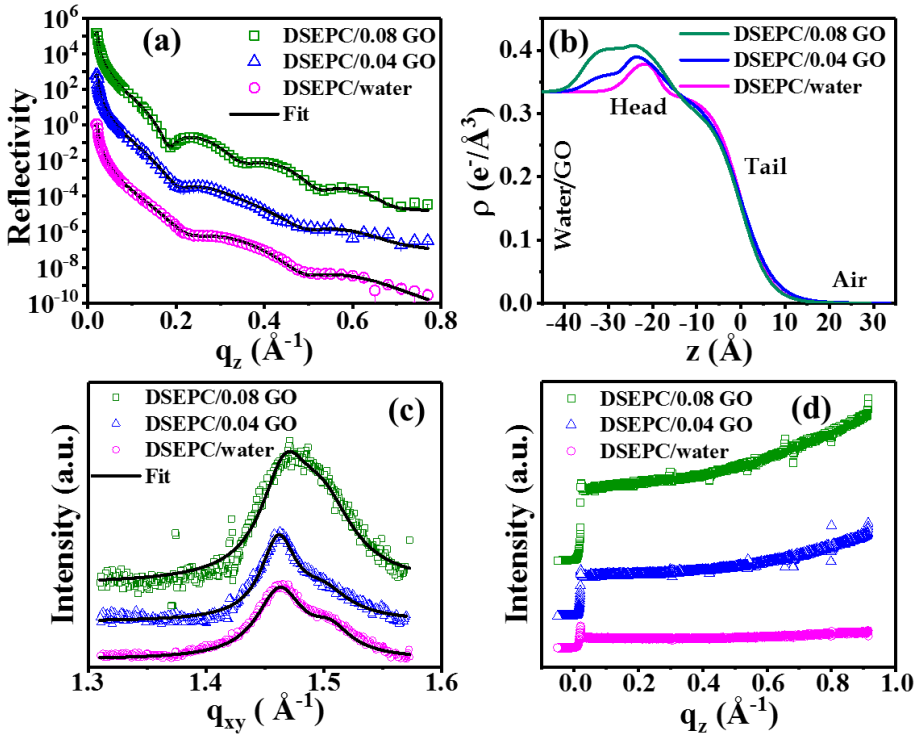

Figure 5. (a) X-ray reflectivity (XRR) profiles of DSEPC monolayer at air-water and air-GO aqueous interface at a surface pressure of 30 mN/m. Symbols represent the experimental data whereas the solid lines indicate fits to the data. (b) Corresponding electron density profile (EDP) obtained from XRR profiles. (c) Background-subtracted diffraction peaks and (d) corresponding Bragg rods obtained from GIXD experiment.

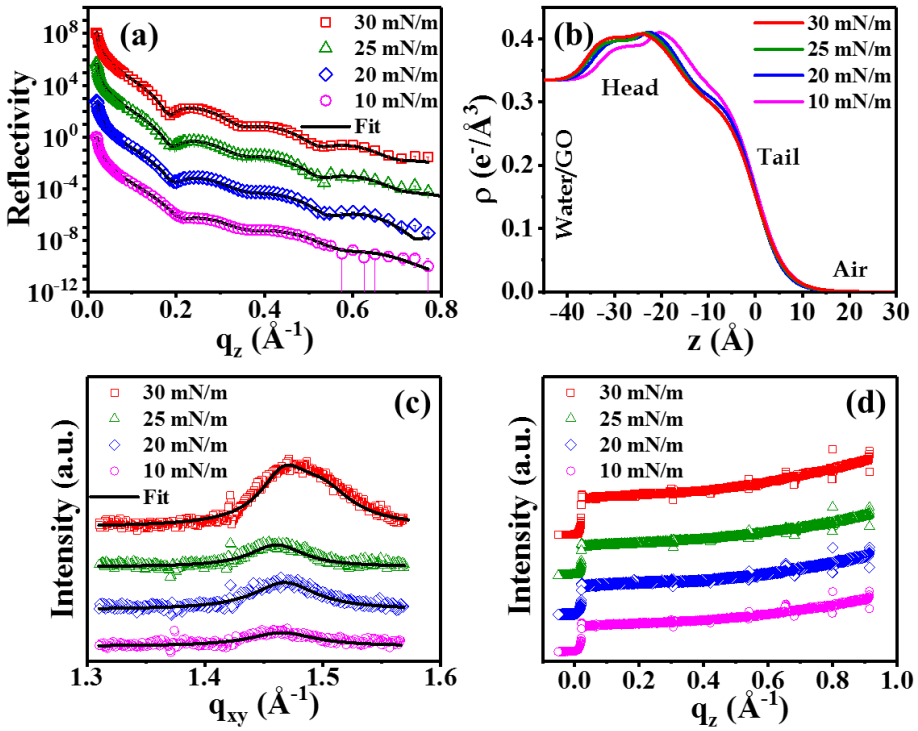

Figure 6. (a) X-ray reflectivity (XRR) profiles from DSEPC monolayers at air-GO aqueous interface (0.08 mg/ml GO dispersion) at different surface pressures. Symbols represent the experimental data whereas the solid lines indicate fits to the data. (b) Corresponding electron density profiles (EDPs) obtained from the best fit of the reflectivity curve. (c) Background-subtracted diffraction peaks and (d) corresponding Bragg rods obtained from GIXD experiment from DSEPC monolayer compressed to different pressures.

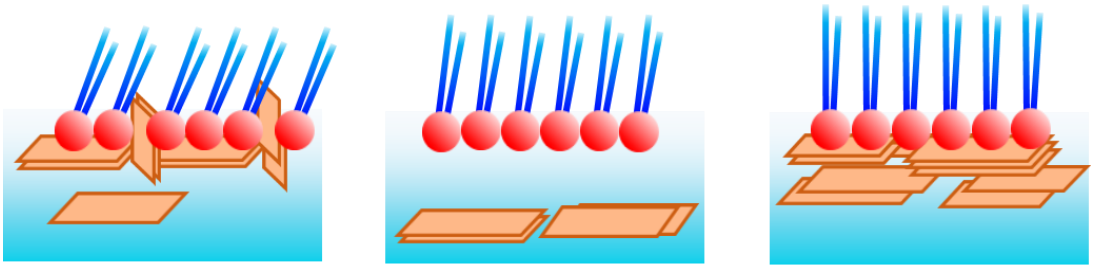

Figure 7. Self-assembly of nano-flakes of graphene oxide (GO) in and around the lipid monolayer. The flakes insert into the zwitterionic lipid film affecting the structure of the whole film. While the negatively charged lipid repel the GO flakes, the positively charged lipid assemble the flakes lying horizontal at the lipid head water interface.

Table 1. Fitted parameters of XRR data for DPPC, DPPG and DSEPC monolayer on subphase of pure water, 0.04 mg/ml GO dispersion and 0.08 mg/ml GO dispersion. All data were obatined at 30 mN/m surface pressure.

Sample	***Subphase***	***Tail***			***Head***			***GO***		
		***d* (Å)**	***ρ* (e^-/Å^3)**	***σ* (Å)**	***d* (Å)**	***ρ* (e/Å^3)**	***σ* (Å)**	***d* (Å)**	***ρ* (e^-/Å^3)**	***σ* (Å)**
DPPC	Water	17.6 ±0.2	0.325 ±0.007	5.0 ±0.1	6.2 ±0.1	0.447 ±0.012	4.0 ±0.2	-	-	-
DPPC	0.04 mg/mL GO	17.8 ±0.2	0.313 ±0.009	4.3 ±0.2	6.8 ±0.2	0.457 ±0.016	5.0 ±0.3	-	-	-
DPPG	Water	18.0 ±0.3	0.322 ±0.011	4.5 ±0.2	8.4 ±0.2	0.439 ±0.015	2.6 ±0.2	-	-	-
DPPG	0.04 mg/mL GO	17.9 ±0.2	0.320 ±0.013	4.4 ±0.1	8.4 ±0.2	0.440 ±0.016	2.7 ±0.2	-	-	-
DSEPC	Water	18.6 ±0.3	0.329 ±0.010	5.8 ±0.3	7.0 ±0.3	0.386 ±0.012	2.0 ±0.1	-	-	-
DSEPC	0.04 mg/mL GO	18.1 ±0.2	0.327 ±0.009	6.7 ±0.3	7.8 ±0.2	0.399 ±0.013	4.4 ±0.2	8.9 ±0.3	0.362 ±0.007	1.7 ±0.1
DSEPC	0.08 mg/mL GO	17.0 ±0.2	0.306 ±0.010	5.8 ±0.2	8.5 ±0.3	0.417 ±0.013	5.0 ±0.3	10.4 ±0.3	0.405 ±0.008	1.4 ±0.1

Table 2. Structural parameters obtained from the GIXD experiments from DPPC, DPPG and DSEPC monolayer on subphase of pure water, 0.04 mg/ml GO dispersion and 0.08 mg/ml GO dispersion. All data were obatined at 30 mN/m surface pressure.

Sample	***Subphase***	***Diffraction peak position*** ($Å^{-1}$) ±0.005 $Å^{-1}$	***d-spacing (Å)*** ±0.05 Å	***Unit cell parameter***		***Area per molecule*** ($Å^2$) ±0.5 ($Å^2$)	***Coherence length*** L_{xy} ***(Å)***	***Coherence length*** L_z ***(Å)***	***Tilt angle*** τ ***(°)***
				Lattice parameter, a (Å) ±0.05 Å	***Angle, γ (°)*** ±1.0°				
DPPC	Water	1.342	d_{10} = 4.68	5.09	113.2	47.7	L_{10} = 70 ±2	19.6 ±0.2	33.5 ±0.2
		1.477	$d_{1\bar{1}}$ = 4.25				$L_{1\bar{1}}$ = 234 ±5		
	0.04 mg/mL GO	1.368	d_{10} = 4.59	5.05	114.5	46.3	L_{10} = 67 ±2	14.5 ±0.3	32.2 ±0.2
		1.480	$d_{1\bar{1}}$ = 4.24				$L_{1\bar{1}}$ = 279 ±4		
DPPG	Water	1.482	d_{10} = 4.24	4.83	118.6	40.9	L_{10} = 210 ±7	19.1 ±0.6	14.7 ±0.2
		1.514	d_{01} = 4.15				L_{01} = 295 ±7		
	0.04 mg/mL GO	1.480	d_{10} = 4.24	4.83	118.5	41.0	L_{10} = 161 ±10	19.2 ±1.0	14.7 ±0.2
		1.514	d_{01} = 4.15				L_{01} = 311 ±6		
DSEPC	Water	1.463	d_{10} = 4.29	4.87	118.1	41.8	L_{10} = 157 ±2	-	-
		1.504	$d_{1\bar{1}}$ = 4.18				$L_{1\bar{1}}$ = 94 ±3		
	0.04 mg/mL GO	1.461	d_{10} = 4.30	4.88	118.2	42.0	L_{10} = 155 ±4	-	-
		1.500	$d_{1\bar{1}}$ = 4.19				$L_{1\bar{1}}$ = 103 ±6		
	0.08 mg/mL GO	1.467	d_{10} = 4.28	4.87	118.5	41.8	L_{10} = 114 ±7	-	-
		1.500	$d_{1\bar{1}}$ = 4.19				$L_{1\bar{1}}$ = 90 ±7		

Table 3. Fitted parameters of XRR data of DSEPC monolayer on subphase of 0.08 mg/ml GO dispersion at different surface pressure.

Sample	***Pressure (mN/m)***	***Tail***			***Head***			***GO***		
		d (Å)	***ρ (e^-/Å^3)***	***σ (Å)***	***d (Å)***	***ρ (e^-/Å^3)***	***σ (Å)***	***d (Å)***	***ρ (e^-/Å^3)***	***σ (Å)***
DSEPC	30	17.0 ±0.2	0.306 ±0.010	5.8 ±0.2	8.5 ±0.3	0.417 ±0.013	5.0 ±0.3	10.4 ±0.3	0.405 ±0.008	1.4 ±0.1
DSEPC	25	16.5 ±0.2	0.304 ±0.009	5.6 ±0.3	8.5 ±0.3	0.419 ±0.012	4.9 ±0.2	10.6 ±0.1	0.399 ±0.007	1.3 ±0.1
DSEPC	20	16.3 ±0.3	0.313 ±0.009	5.4 ±0.2	7.8 ±0.2	0.418 ±0.012	4.1 ±0.2	10.5 ±0.2	0.400 ±0.009	1.3 ±0.1
DSEPC	10	14.7 ±0.3	0.329 ±0.010	5.7 ±0.2	7.6 ±0.2	0.419 ±0.010	4.2 ±0.2	10.9 ±0.2	0.390 ±0.009	1.4 ±0.1

Table 4. Structural parameters obtained from the GIXD data of DSEPC monolayer at air/0.08 mg/ml GO aqueous interface as a function of surface pressure.

Surface pressure (mN/m)	***Diffraction peak position (Å^{-1})*** ±0.005 Å^{-1}	***d-spacing (Å)*** ±0.05 Å	***Unit cell parameter***		***Area per chains (Å^2)*** ±0.5 (Å^2)	***Coherence length L_{xy} (Å)***
			Lattice parameter, a (Å) ±0.05 Å	***Angle, γ (°)*** ±1.0°		
30	1.467	d_{10} = 4.28	4.87	118.5	41.8	L_{10} = 114±7
	1.500	$d_{1\bar{1}}$ = 4.19				$L_{1\bar{1}}$ = 90±7
25	1.461	d_{10} = 4.30	4.96	120	42.6	L_{10} = 82±4
20	1.468	d_{10} = 4.28	4.94	120	42.2	L_{10} = 86±3
10	1.465	d_{10} = 4.29	4.95	120	42.4	L_{10} = 101±5

REFERENCES

1. Geim, A. K.; Novoselov, K. S., The Rise of Graphene. In *Nanoscience and Technology: A Collection of Reviews from Nature Journals*, World Scientific: **2010**; pp 11-19.

2. Vimalanandan, A.; Lv, L. P.; Tran, T. H.; Landfester, K.; Crespy, D.; Rohwerder, M., Redox-Responsive Self-Healing for Corrosion Protection. *Advanced Materials* **2013**, *25*, 6980-6984.

3. Compton, O. C.; Nguyen, S. T., Graphene Oxide, Highly Reduced Graphene Oxide, and Graphene: Versatile Building Blocks for Carbon-Based Materials. *Small* **2010**, *6*, 711-723.

4. Tao, Y.; Lin, Y.; Huang, Z.; Ren, J.; Qu, X., Incorporating Graphene Oxide and Gold Nanoclusters: A Synergistic Catalyst with Surprisingly High Peroxidase-Like Activity over a Broad Ph Range and Its Application for Cancer Cell Detection. *Advanced materials* **2013**, *25*, 2594-2599.

5. Morales-Narváez, E.; Merkoçi, A., Graphene Oxide as an Optical Biosensing Platform. *Advanced Materials* **2012**, *24*, 3298-3308.

6. Liu, Z.; Robinson, J. T.; Sun, X.; Dai, H., Pegylated Nanographene Oxide for Delivery of Water-Insoluble Cancer Drugs. *Journal of the American Chemical Society* **2008**, *130*, 10876-10877.

7. Tian, B.; Wang, C.; Zhang, S.; Feng, L.; Liu, Z., Photothermally Enhanced Photodynamic Therapy Delivered by Nano-Graphene Oxide. *ACS nano* **2011**, *5*, 7000-7009.

8. Li, M.; Yang, X.; Ren, J.; Qu, K.; Qu, X., Using Graphene Oxide High near-Infrared Absorbance for Photothermal Treatment of Alzheimer's Disease. *Advanced Materials* **2012**, *24*, 1722-1728.

9. Akhavan, O.; Ghaderi, E., Toxicity of Graphene and Graphene Oxide Nanowalls against Bacteria. *ACS nano* **2010**, *4*, 5731-5736.

10. Liu, S.; Zeng, T. H.; Hofmann, M.; Burcombe, E.; Wei, J.; Jiang, R.; Kong, J.; Chen, Y., Antibacterial Activity of Graphite, Graphite Oxide, Graphene Oxide, and Reduced Graphene Oxide: Membrane and Oxidative Stress. *ACS nano* **2011**, *5*, 6971-6980.

11. Nurunnabi, M.; Parvez, K.; Nafiujjaman, M.; Revuri, V.; Khan, H. A.; Feng, X.; Lee, Y.-k., Bioapplication of Graphene Oxide Derivatives: Drug/Gene Delivery, Imaging, Polymeric Modification, Toxicology, Therapeutics and Challenges. *RSC advances* **2015**, *5*, 42141-42161.

12. Giri, R.; Mukhopadhyay, M.; Basak, U.; Chakrabarti, A.; Sanyal, M.; Runge, B.; Murphy, B., Continuous Uptake or Saturation—Investigation of Concentration and Surface-Packing-Specific Hemin Interaction with Lipid Membranes. *The Journal of Physical Chemistry B* **2018**, *122*, 7547-7554.

13. Novoselov, K. S.; Geim, A. K.; Morozov, S. V.; Jiang, D.; Zhang, Y.; Dubonos, S. V.; Grigorieva, I. V.; Firsov, A. A., Electric Field Effect in Atomically Thin Carbon Films. *Science* **2004**, *306*, 666-669.

14. Reina, G.; González-Domínguez, J. M.; Criado, A.; Vázquez, E.; Bianco, A.; Prato, M., Promises, Facts and Challenges for Graphene in Biomedical Applications. *Chemical Society Reviews* **2017**, *46*, 4400-4416.

15. Perreault, F.; De Faria, A. F.; Elimelech, M., Environmental Applications of Graphene-Based Nanomaterials. *Chemical Society Reviews* **2015**, *44*, 5861-5896.

16. Wu, L.; Zeng, L.; Jiang, X., Revealing the Nature of Interaction between Graphene Oxide and Lipid Membrane by Surface-Enhanced Infrared Absorption Spectroscopy. *Journal of the American Chemical Society* **2015**, *137*, 10052-10055.

17. Chen, J.; Zhou, G.; Chen, L.; Wang, Y.; Wang, X.; Zeng, S., Interaction of Graphene and Its Oxide with Lipid Membrane: A Molecular Dynamics Simulation Study. *The Journal of Physical Chemistry C* **2016**, *120*, 6225-6231.

18. Puigpelat, E.; Ignés-Mullol, J.; Sagués, F.; Reigada, R., Interaction of Graphene Nanoparticles and Lipid Membranes Displaying Different Liquid Orderings: A Molecular Dynamics Study. *Langmuir* **2019**, *35*, 16661-16668.

19. Zhang, X.; Cao, F.; Wu, L.; Jiang, X., Understanding the Synergic Mechanism of Weak Interactions between Graphene Oxide and Lipid Membrane Leading to the Extraction of Lipids. *Langmuir* **2019**, *35*, 14098-14107.

20. Frost, R.; Jönsson, G. E.; Chakarov, D.; Svedhem, S.; Kasemo, B., Graphene Oxide and Lipid Membranes: Interactions and Nanocomposite Structures. *Nano letters* **2012**, *12*, 3356-3362.

21. Li, S.; Stein, A. J.; Kruger, A.; Leblanc, R. M., Head Groups of Lipids Govern the Interaction and Orientation between Graphene Oxide and Lipids. *The Journal of Physical Chemistry C* **2013**, *117*, 16150-16158.

22. Mandal, P.; Bhattacharya, G.; Bhattacharyya, A.; Roy, S. S.; Ghosh, S. K., Unravelling the Structural Changes of Phospholipid Membranes in Presence of Graphene Oxide. *Applied Surface Science* **2020**, 148252.

23. Sanyal, S.; Menon, A. K., Flipping Lipids: Why An'what's the Reason For? *ACS chemical biology* **2009**, *4*, 895-909.

24. Oliver, A. E.; Parikh, A. N., Templating Membrane Assembly, Structure, and Dynamics Using Engineered Interfaces. *Biochimica et Biophysica Acta (BBA)-Biomembranes* **2010**, *1798*, 839-850.

25. Hummers, W., Offeman, Re,"Preparation of Graphitic Oxide". *J. Am. Chem. Soc* **1958**, *80*, 1339.

26. Marcano, D. C.; Kosynkin, D. V.; Berlin, J. M.; Sinitskii, A.; Sun, Z.; Slesarev, A.; Alemany, L. B.; Lu, W.; Tour, J. M., Improved Synthesis of Graphene Oxide. *ACS nano* **2010**, *4*, 4806-4814.

27. Morini, M. A.; Sierra, M. B.; Pedroni, V. I.; Alarcon, L. M.; Appignanesi, G. A.; Disalvo, E. A., Influence of Temperature, Anions and Size Distribution on the Zeta Potential of Dmpc, Dppc and Dmpe Lipid Vesicles. *Colloids and Surfaces B: Biointerfaces* **2015**, *131*, 54-58.

28. Mitra, S.; Ray, D.; Bhattacharya, G.; Gupta, R.; Sen, D.; Aswal, V.; Ghosh, S., Probing the Effect of a Room Temperature Ionic Liquid on Phospholipid Membranes in Multilamellar Vesicles. *European Biophysics Journal* **2019**, *48*, 119-129.

29. Smith, M. C.; Crist, R. M.; Clogston, J. D.; McNeil, S. E., Zeta Potential: A Case Study of Cationic, Anionic, and Neutral Liposomes. *Analytical and bioanalytical chemistry* **2017**, *409*, 5779-5787.

30. Kjaer, K.; Als-Nielsen, J.; Helm, C.; Tippman-Krayer, P.; Moehwald, H., Synchrotron X-Ray Diffraction and Reflection Studies of Arachidic Acid Monolayers at the Air-Water Interface. *The Journal of Physical Chemistry* **1989**, *93*, 3200-3206.

31. Helm, C.; Möhwald, H.; Kjaer, K.; Als-Nielsen, J., Phospholipid Monolayers between Fluid and Solid States. *Biophysical journal* **1987**, *52*, 381-390.

32. Kjaer, K.; Als-Nielsen, J.; Helm, C.; Laxhuber, L.; Möhwald, H., Ordering in Lipid Monolayers Studied by Synchrotron X-Ray Diffraction and Fluorescence Microscopy. *Physical review letters* **1987**, *58*, 2224.

33. Basu, J.; Sanyal, M. K., Ordering and Growth of Langmuir–Blodgett Films: X-Ray Scattering Studies. *Physics Reports* **2002**, *363*, 1-84.

34. Murphy, B. M.; Greve, M.; Runge, B.; Koops, C. T.; Elsen, A.; Stettner, J.; Seeck, O. H.; Magnussen, O. M., A Novel X-Ray Diffractometer for Studies of Liquid–Liquid Interfaces. *Journal of synchrotron radiation* **2014**, *21*, 45-56.

35. Dietrich, S.; Haase, A., Scattering of X-Rays and Neutrons at Interfaces. *Physics Reports* **1995**, *260*, 1-138.

36. Parrat, L., Surface Studies Ofsolids by Total Reflexion of X-Rays. *Phys. Rev* **1954**, *95*, 359-369.

37. Als-Nielsen, J.; McMorrow, D., *Elements of Modern X-Ray Physics*; John Wiley & Sons, **2011**.

38. Helm, C.; Möhwald, H.; Kjaer, K.; Als-Nielsen, J., Phospholipid Monolayer Density Distribution Perpendicular to the Water Surface. A Synchrotron X-Ray Reflectivity Study. *EPL (Europhysics Letters)* **1987**, *4*, 697.

39. Jensen, T. R.; Kjær, K., Structural Properties and Interactions of Thin Films at the Air-Liquid Interface Explored by Synchrotron X-Ray Scattering. *Novel methods to study interfacial layers* **2001**, *11*, 2054.

40. Stefaniu, C.; Brezesinski, G., Grazing Incidence X-Ray Diffraction Studies of Condensed Double-Chain Phospholipid Monolayers Formed at the Soft Air/Water Interface. *Advances in colloid and interface science* **2014**, *207*, 265-279.

41. Pignat, J.; Daillant, J.; Leiserowitz, L.; Perrot, F., Grazing Incidence X-Ray Diffraction on Langmuir Films: Toward Atomic Resolution. *The Journal of Physical Chemistry B* **2006**, *110*, 22178-22184.

42. Broniatowski, M.; Flasiński, M.; Dynarowicz-Łątka, P.; Majewski, J., Grazing Incidence Diffraction and X-Ray Reflectivity Studies of the Interactions of Inorganic Mercury Salts with Membrane Lipids in Langmuir Monolayers at the Air/Water Interface. *The Journal of Physical Chemistry B* **2010**, *114*, 9474-9484.

43. Scherrer, P., Bestimmung Der Inneren Struktur Und Der Größe Von Kolloidteilchen Mittels Röntgenstrahlen. In *Kolloidchemie Ein Lehrbuch*, Springer: **1912**; pp 387-409.

44. Patterson, A., The Scherrer Formula for X-Ray Particle Size Determination. *Physical review* **1939**, *56*, 978.

45. Sabatini, K.; Mattila, J.-P.; Kinnunen, P. K., Interfacial Behavior of Cholesterol, Ergosterol, and Lanosterol in Mixtures with Dppc and Dmpc. *Biophysical journal* **2008**, *95*, 2340-2355.

46. Hwang, M.-J.; Kim, K., Poly (Ethylenimine) as a Subphase Stabilizer of Stearic Acid Monolayers at the Air/Water Interface: Surface Pressure− Area Isotherm and Infrared Spectroscopy Study. *Langmuir* **1999**, *15*, 3563-3569.

47. Giri, R. P.; Chakrabarti, A.; Mukhopadhyay, M. K., Cholesterol-Induced Structural Changes in Saturated Phospholipid Model Membranes Revealed through X-Ray Scattering Technique. *The Journal of Physical Chemistry B* **2017**, *121*, 4081-4090.

48. Ariga, K.; Mori, T.; Li, J., Langmuir Nanoarchitectonics from Basic to Frontier. *Langmuir* **2018**, *35*, 3585-3599.

49. Ariga, K., Don't Forget Langmuir–Blodgett Films 2020: Interfacial Nanoarchitectonics with Molecules, Materials, and Living Objects. *Langmuir* **2020**, *36*, 7158-7180.

50. Birdi, K., *Self-Assembly Monolayer Structures of Lipids and Macromolecules at Interfaces*; Springer Science & Business Media, **2006**.

51. Baoukina, S.; Monticelli, L.; Marrink, S. J.; Tieleman, D. P., Pressure− Area Isotherm of a Lipid Monolayer from Molecular Dynamics Simulations. *Langmuir* **2007**, *23*, 12617-12623.

52. Bonatout, N.; Muller, F.; Fontaine, P.; Gascon, I.; Konovalov, O.; Goldmann, M., How Exfoliated Graphene Oxide Nanosheets Organize at the Water Interface: Evidence for a Spontaneous Bilayer Self-Assembly. *Nanoscale* **2017**, *9*, 12543-12548.

53. Geraldo, V. P.; Pavinatto, F. J.; Nobre, T. M.; Caseli, L.; Oliveira Jr, O. N., Langmuir Films Containing Ibuprofen and Phospholipids. *Chemical Physics Letters* **2013**, *559*, 99-106.

54. Miller, C.; Busath, D.; Strongin, B.; Majewski, J., Integration of Ganglioside Gt1b Receptor into Dppe and Dppc Phospholipid Monolayers: An X-Ray Reflectivity and Grazing-Incidence Diffraction Study. *Biophysical journal* **2008**, *95*, 3278-3286.

55. Majewski, J.; Stec, B., X-Ray Scattering Studies of Model Lipid Membrane Interacting with Purothionin Provide Support for a Previously Proposed Mechanism of Membrane Lysis. *European Biophysics Journal* **2010**, *39*, 1155-1165.

56. Vineyard, G. H., Grazing-Incidence Diffraction and the Distorted-Wave Approximation for the Study of Surfaces. *Physical Review B* **1982**, *26*, 4146.

57. Wydro, P.; Flasiński, M.; Broniatowski, M., Molecular Organization of Bacterial Membrane Lipids in Mixed Systems—a Comprehensive Monolayer Study Combined with Grazing Incidence X-Ray Diffraction and Brewster Angle Microscopy Experiments. *Biochimica et Biophysica Acta (BBA)-Biomembranes* **2012**, *1818*, 1745-1754.

58. Neville, F.; Ishitsuka, Y.; Hodges, C. S.; Konovalov, O.; Waring, A. J.; Lehrer, R.; Lee, K. Y. C.; Gidalevitz, D., Protegrin Interaction with Lipid Monolayers: Grazing Incidence X-Ray Diffraction and X-Ray Reflectivity Study. *Soft matter* **2008**, *4*, 1665-1674.

59. Bhattacharya, G.; Mitra, S.; Mandal, P.; Dutta, S.; Giri, R.; Ghosh, S., Thermodynamics of Interaction of Ionic Liquids with Lipid Monolayer. *Biophysical reviews* **2018**, *10*, 709-719.

60. Zhang, P.; Villanueva, V.; Kalkowski, J.; Liu, C.; Donovan, A. J.; Bu, W.; Schlossman, M. L.; Lin, B.; Liu, Y., Molecular Interactions of Phospholipid Monolayers with a Model Phospholipase. *Soft matter* **2019**, *15*, 4068-4077.

61. Mitra, S.; Das, R.; Singh, A.; Mukhopadhyay, M. K.; Roy, G.; Ghosh, S. K., Surface Activities of a Lipid Analogue Room-Temperature Ionic Liquid and Its Effects on Phospholipid Membrane. *Langmuir* **2019**, *36*, 328-339.

62. Dreyer, D.; Park, S.; Bielawski, C.; Ruoff, R., The Chemistry of Go Chem. *Soc. Rev* **2010**, *39*, 228-40.

63. Eda, G.; Fanchini, G.; Chhowalla, M., Large-Area Ultrathin Films of Reduced Graphene Oxide as a Transparent and Flexible Electronic Material. *Nature nanotechnology* **2008**, *3*, 270-274.

64. Lei, H.; Zhou, X.; Wu, H.; Song, Y.; Hu, J.; Guo, S.; Zhang, Y., Morphology Change and Detachment of Lipid Bilayers from the Mica Substrate Driven by Graphene Oxide Sheets. *Langmuir* **2014**, *30*, 4678-4683.

65. Mohanty, N.; Berry, V., Graphene-Based Single-Bacterium Resolution Biodevice and DNA Transistor: Interfacing Graphene Derivatives with Nanoscale and Microscale Biocomponents. *Nano letters* **2008**, *8*, 4469-4476.

66. Kim, H.; Namgung, R.; Singha, K.; Oh, I.-K.; Kim, W. J., Graphene Oxide–Polyethylenimine Nanoconstruct as a Gene Delivery Vector and Bioimaging Tool. *Bioconjugate chemistry* **2011**, *22*, 2558-2567.

67. Yang, Y.; Asiri, A. M.; Tang, Z.; Du, D.; Lin, Y., Graphene Based Materials for Biomedical Applications. *Materials today* **2013**, *16*, 365-373.

68. Chau, N. D. Q.; Reina, G.; Raya, J.; Vacchi, I. A.; Ménard-Moyon, C.; Nishina, Y.; Bianco, A., Elucidation of Sirna Complexation Efficiency by Graphene Oxide and Reduced Graphene Oxide. *Carbon* **2017**, *122*, 643-652.

69. Zhang, L.; Xu, B.; Wang, X., Cholesterol Extraction from Cell Membrane by Graphene Nanosheets: A Computational Study. *The Journal of Physical Chemistry B* **2016**, *120*, 957-964.

70. Van Meer, G.; Voelker, D. R.; Feigenson, G. W., Membrane Lipids: Where They Are and How They Behave. *Nature reviews Molecular cell biology* **2008**, *9*, 112-124.

71. Cooper, G. M., The Cell: A Molecular Approach 2nd Edition. National Center for Biotechnology InformationÕs Bookshelf: **2000**.

72. Bhattacharya, G.; Giri, R.; Saxena, H.; Agrawal, V.; Gupta, A.; Mukhopadhyay, M.; Ghosh, S., X-Ray Reflectivity Study of the Interaction of an Imidazolium-Based Ionic Liquid with a Soft Supported Lipid Membrane. *Langmuir* **2017**, *33*, 1295-1304.

Table of Content